Electrodeposited Superconducting Re on Flexible Substrates Using Aerosol Jet Printed Metal Seed Layers

Kamal Ahammed , Lok-Kun Tsui , Shianne Carroll, Judi Lavin, Member, IEEE, and Qiang Huang

Abstract—Electrodeposition of superconducting Re on aerosol jet printed (AJP) metal seed layers on a flexible substrate is investigated. Silver and gold seed layers are printed using the "Nanojet" aerosol jet printer on Kapton films. Thermogravimetric analysis, stylus profilometer, and three-point bend test are performed to characterize the AJP metal seed layer on such flexible substrates. Electrodeposition of Re is successfully carried out on the Au seed layer and is characterized using various techniques, such as X-ray fluorescence spectroscopy, focused ion beam, scanning electron microscope, energy dispersive spectroscopy, X-ray diffraction, and four-point probe electrical measurements at cryogenic temperatures. The superconductivity of such a flexible Re stack is confirmed with an elevated critical temperature (T_c) of 6 K.

Index Terms—Aerosol jet printing, electrodeposition, flexible interconnects, superconductivity.

I. INTRODUCTION

UANTUM computers aim to solve a range of limitations currently unachievable with conventional computing technology. The applications include physics and chemistry simulations, cryptography, machine learning, and computational tasks in the fields of medicine and finance [1], [2], [3], [4], [5]. One of the mainstream and most developed platforms of quantum computers is based on qubits implemented with superconducting Josephson junctions operated at 10 mK or below in a dilution refrigerator [6]. In this platform, communications between the qubits and other control electronics operated at room temperature or other various temperatures

Manuscript received 15 February 2023; revised 3 July 2023; accepted 28 August 2023. Date of publication 1 September 2023; date of current version 21 September 2023. This work was supported in part by Sandia National Laboratories (a multimission laboratory managed and operated by National Technology & Engineering Solutions of Sandia, LLC, a wholly owned subsidiary of Honeywell International Inc., for the U.S. Department of Energy's National Nuclear Security Administration under Contract DE-NA0003525) and in part by the National Science Foundation under Grant 2016541. (Corresponding author: Oiang Huang.)

Kamal Ahammed and Qiang Huang are with the Department of Chemical and Biological Engineering, University of Alabama, Tuscaloosa, AL 35487 USA (e-mail: kahammed@crimson.ua.edu; qhuang@eng.ua.edu).

Lok-Kun Tsui is with the Center for Micro-Engineered Materials, The University of New Mexico, Albuquerque, NM 87123 USA, and also with the Sandia National Laboratories, Albuquerque, NM 87123 USA (e-mail: Itsui@sandia.gov).

Shigns Carrell and India Lapin page with Sandia National Laboratories Albuquerque, NM 87123 USA (e-mail: Itsui@sandia.gov).

Shianne Carroll and Judi Lavin are with Sandia National Laboratories, Albuquerque, NM 87123 USA (e-mail: shicarr@sandia.gov; jlavin@sandia.gov).

This article has supplementary material provided by the authors and color versions of one or more figures available at https://doi.org/10.1109/TASC.2023.3311320.

Digital Object Identifier 10.1109/TASC.2023.3311320

are achieved with a chandelier of stainless-steel coaxial cables that must be connected individually [6]. The joule heating generated in any of these connection cables undermines the efficiency of the overall refrigeration system. This is particularly significant as the dilution refrigeration power quickly diminishes as the temperature decreases. As a result, not only is the operation fidelity of qubits compromised by thermal perturbation but also the number of qubits that can be operated simultaneously and the functionality of qubit circuits are limited.

Using superconducting interconnects in the form of flexible ribbon cable would not only simplify the assembly but also eliminate the concern of joule heating. Ideally, a superconducting critical temperature (T_c) above 4.2 K would be preferred to enable its operation in the liquid helium stages. Recently reported methods of patterning superconductors on flexible substrates include Ga-In-Sn and NbSe₂ by inkjet [7], [8], Nb and its alloys by sputtering and photolithography [9], and YBCO on Kapton by an adhesive transfer method [10]. Aerosol iet printing is an attractive method to pattern electronic devices because of its low cost compared with clean-room lithography techniques, rapid printing rate, sub-10 µm resolution, and compatibility with a wide range of conductor and insulator materials [11]. More importantly, it allows the formation of arbitrary patterns in a continuous manufacturing fashion. These two features are well matched by the self-alignment nature and continuous operation of electrodeposition. Furthermore, electrodeposition is considered a cost-effective, controllable, scalable, and facile process for material deposition [12] and has been widely used in device fabrication [13], [14], [15]. Recently, the electrodeposition of Cu and Ni microstructures using the AJP metal seed layer has been reported [16].

Electrodeposited amorphous Re has a critical temperature between 5 and 6 K, rendering it a promising superconductor compatible with liquid He cryogen [17], [18]. In addition, the adoption of the so-called water-in-salt electrolytes in Re electrodeposition suppresses the concomitant hydrogen evolution, thus reducing the film cracks and improving the film morphology without compromising the critical temperature [18], [19], [20]. While electrodeposition of superconducting oxides on flexible metal foils has been attempted [21], [22], [23], the electrodeposition step typically produces metal and metal hydroxide precursors, which are subsequently converted into the final superconductor using high-temperature annealing at

1051-8223 © 2023 IEEE. Personal use is permitted, but republication/redistribution requires IEEE permission. See https://www.ieee.org/publications/rights/index.html for more information.

beyond $700\,^{\circ}\text{C}$. Such thermal processes are not compatible with polymer-based flexible substrates.

In this study, we investigate the superconducting behavior of Re on AJP metal seed layers (Ag and Au) on flexible Kapton substrates for the advancement of superconducting interconnect technologies. This combined approach would not only eliminate the aforementioned key roadblocks in the scaling and fidelity of quantum computing but also offer the freedom of connection design to enable new operations or functionalities of quantum circuits.

II. EXPERIMENTAL

A Nanojet aerosol printing system from Integrated Deposition Solutions is used to deposit metal seed layers (Au and Ag) on Kapton. The operation principle and configuration of the AJP are reported in an earlier work [16]. The highly flexible, stable, and temperature-resistant polyimide substrate, or Kapton films, with a thickness of 127 μm are acquired from Granger. Kapton films are used as received (AR) or after being roughened using sandpapers with different grit numbers from 320 to 1200. Before AJP of seed metals, all Kapton films, regardless of the roughening procedure, are cleaned with sonication in isopropyl alcohol for 15 min. Both Ag and Au are chosen as the seed metals for the study because of their high conductivity, easiness, and prior knowledge of the AJP process.

Ag40X and Au40X colloidal nanoparticle suspensions in xylenes conductive nanoink, both acquired from UTDots, are used in this work. The AR inks are reformulated to optimize the printed ink resolution as identified in previous work [16]: Ag40X 20 vol%, terpineol 20 vol%, and xylenes 60 vol% for Ag ink formula; and Au40X 40 vol%, terpineol 20 vol%, and xylenes 40 vol% for Au ink formula. All printing is carried out with a travel speed of 300 mm/min and four-layer depositions with a platen temperature of 100 °C. A Lennox Laser 750 μm orifice first focusing lens and a Fisnar 160 µm Micron-S Precision second focusing tip are used to collimate the ink stream for all prints. Print head deposition conditions are optimized for each material. The optimized deposition conditions for Ag are: atomizer voltage 18 V, aerosol gas 4.0 SCCM, and sheath gas 40 SCCM. The optimized conditions for Au are: atomizer voltage 20 V, aerosol gas 4.0 SCCM, and sheath gas 40 SCCM. In both metal cases, the sheath gas is passed through a glass jar containing xylenes to prevent the aerosolized ink from drying out. The printed ink patterns on Kapton are sintered in an oven under atmospheric conditions at 120 °C for 3 h for Ag and 300 °C for 3 h for Au to drive off organics, allowing particle coalescence, which ultimately renders the materials conductive.

Thermogravimetric analysis is performed on reformulated inks using a Netzsch STA 490C/CH for Ag40X and a TA Instruments SDT 2960 for Au40X. Both inks are characterized in an air atmosphere at a ramp rate of 1 $^{\circ}\text{C/min}$. A Bruker Dektat stylus profilometer with a 2 μm tip size is used to determine the thickness of AJP seed layer on Kapton. Optical micrographs are acquired on Keyence VH-Z100R and VH-Z00R optical microscopes. Adhesion tests of the AJP seed metal and the seed

metal-rhenium composite on Kapton are carried out according to the ASTM D3359 Tape Test protocol [24].

Flexure tests are carried out on samples approximately 4 mm wide and 15 mm long. Three-point bend tests are conducted in an RSA G2 solids analyzer from TA Instruments with a 10 mm support span fixture. The samples are tested first with the printed Ag/Au side face up, then retested with the printed side face down. Samples are tested at a strain rate of 0.1 mm/mm/min as recommended in ASTM D790 while the axial load is recorded. The tests are terminated on passing through the yield point, which is seen on a stress-strain curve as the maximum stress and corresponding strain. Upon completion of three-point bend testing, the samples are reused for cyclic bend testing in a three-point bend orientation using the same instrument setup. Samples are tested with the printed Ag/Au side face down. A maximum strain of 1.27% is applied at a frequency of 1/30 Hz, which corresponds with the same strain rate in the three-point bend tests. The test runs for 200 cycles and measures the axial load during bending.

A three-component electrochemical cell is used to deposit Re on the printed seed layers. A 99.99% platinum (Pt) foil is used as the anode and an Ag/AgCl electrode with saturated KCl is used as the reference. All potentials in this study are reported with respect to this reference. A custom-made holder with a rotating disc electrode configuration is used as the cathode. The Kapton substrates with metal seed are mounted on this holder, which rotates to provide solution agitation. An Autolab 302N potentiostat from Metrohm is used to control the electrical current and voltage for electrodeposition. A typical AJP metal (Ag or Au) pattern includes a $1 \text{ mm} \times 10 \text{ mm}$ bar and a $2 \text{ mm} \times 2 \text{ mm}$ pad. The bar pattern is used to deposit Re films for electrical and superconductivity characterization. A contact pin lands on the pad and forms the electrical connectivity with the potentiostat for electrodeposition. The electrodeposited Re typically covers the entire metal pattern except for a circular footprint of the contact pin on the pad.

Re electrodeposition is carried out using a so-called "waterin-salt" electrolyte, where a superhigh concentration of salt is present to deplete the free water molecules and suppress the hydrogen evolution side reactions [20]. More specifically, the electrolyte comprises 25 mM NH₄ReO₄ as the Re source, 0.1 M H₂SO₄ to provide an acidic environment for the deposition, and 5 M LiCl to deplete free water molecules. All chemicals are of ACS reagent grade and deionized (DI) water with a resistivity of $18.2 \text{M}\Omega \cdot \text{cm}$ is used for electrolyte preparation. Detailed electrochemical studies of Re deposition in such electrolytes have been published separately [19]. Re films in this study are electrodeposited at a constant potential of $-1 \, \text{V}$ and a fixed rotation rate of 400 r/min. The deposition time is fixed at 300s unless otherwise mentioned. The Re film thickness varies between 400 and 500 nm due to a small variation of the overall ohmic resistance of the circuit between experiments. Re films are rinsed with DI water immediately after electrodeposition followed by air blow dry.

The thickness of electrodeposited Re is determined using a Bruker M1 Mistral X-ray fluorescence (XRF) spectroscope with a 0.7mm collimator and 50kV excitation voltage. The

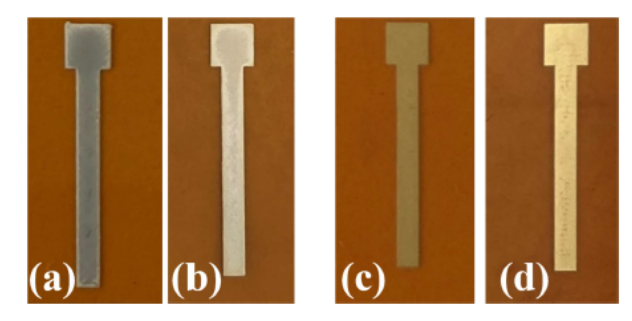


Fig. 1. Optical images of AJP (a) and (b) Ag and (c) and (d) Au on $127\,\mu m$ thick (a) and (c) smooth Kapton and (b) and (d) Kapton films roughened with 1200 grit sandpaper.

morphology of electrodeposited Re films is characterized using a Thermal Scientific Apero field emission scanning electron microscope (SEM) equipped with a Bruker energy dispersive X-ray spectrometer (EDS). The latter is used to acquire the elemental mapping to characterize the uniformity or coverage of the deposited Re. It is also used to characterize the cross-section of the film stack on Kapton. In this latter case, an FEI quanta focus ion beam (FIB) station is used to section and polish the film stack. Crystallographic characterization of the films is carried out using a Bruker D8 powder diffractometer (XRD) with Co K_{α} source (wavelength = 1.79 Å), operated at 40 kV and 35 mA. The electrical resistance of the AJP seed layer and the fully deposited film stack are determined using a four-point probe setup on the bar pattern with a current source and microvoltameter. The superconducting transition temperature or the critical temperature (T_c) of the electrodeposited Re films on a flexible substrate is measured using a Quantum Design Dynacool Physical Property Measurement System (PPMS) with a dc current of 1 mA. This transition is determined by recording the film resistance along with a temperature sweep from 30 K down to 1.8 K. A four-probe configuration is used for the resistance measurement, where Dupont 4929N silver paint and aluminum wires are used to form the connections between the deposited film and the resistivity puck for PPMS.

III. RESULT AND DISCUSSION

A. Adhesion Studies

Fig. 1 shows an optical inspection of the typical Ag and Au patterns printed on both smooth and roughened Kapton films postsintering. Tape tests are also carried out according to ASTM D3359 protocol and the results are shown in Supplemental Information.

While the Ag patterns, sintered at 120 °C for 3 h after AJ printing on both smooth and roughened Kapton, show good adhesion in Fig. S1, complete delamination post Re electrodeposition is observed in Figs. 2 and S2. This delamination occurs regardless of modification of deposition voltage and the use of a pulse scheme. The latter is often used to lower the residual stress of film [25]. In addition, reducing the acidity of Re electrolytes is also found of little help in improving the adhesion. For this reason, no efforts are taken to evaluate the adhesion of Re on AJP Ag on Kapton. A higher sintering temperature (300 °C) appears









Fig. 2. Optical images of about 400-nm Re electrodeposited on (a) and (b) Ag and (c) and (d) Au seed layers AJP on (a) and (c) smooth and (b) and (d) 1200 grit roughened Kapton.

to aggravate the adhesion of Ag on Kapton, as shown in Fig. S3(b) and (d). Further microscopic investigations will be needed to understand the surface interactions at different temperatures.

A good ASTM adhesion rating is also observed for AJP Au on 127 μm -thick Kapton sintered at 300 °C for 3 h, both smooth and roughened (see Fig. S4). In contrast to Ag, excellent adhesion is also achieved postelectrodeposition of Re with no delamination observed as shown in Fig. 2(c) and (d). The detailed results of ASTM D3359 tape tests are presented as Fig. S5 in Supplemental Information, where almost no delamination is observed on roughened Kapton and slight delamination on smooth Kapton. It is worth noting that this much-improved adhesion sustains even when the Re film thickness increases over five times from under 500 nm to over 2.6 μm . The films with different thicknesses for adhesion comparison are electrodeposited at the same voltage $(-1\,V\,$ versus Ag/AgCl) and rotation rate (400 r/min) using a longer deposition time.

B. Cross-Sectional Characterization

Because the metal stack with Ag seed delaminates from the Kapton substrate upon Re electrodeposition and prevents further characterization, cross-sectional characterization is only performed before Re deposition for printed Ag. Fig. 3(a) and (b) shows the SEM images of a FIB prepared section within the Ag pattern. A clear adherent interface is observed between Ag and Kapton with no delamination. The Kapton substrate of the specimen is roughened with 1200 grit sandpaper, which corresponds to the topography of the film, or the waviness of the interface observed in the images. The Ag layer is printed with four layers, where each layer approximately corresponds to a quarter of the total thickness. But no difference between these paths or no clear indication of lamination is observed in the cross section of these sintered Ag patterns. Another cross section is prepared by cleaving the film with a knife blade and polishing the edge surface with FIB, and the SEM image is presented in Fig. 3(c). A clear delamination is observed with a gap between the metal film and the Kapton substrate, which is probably created during the knife cleaving. The Ag X-ray signal from an EDS line scan is also included in the image to confirm this crevice.

A similar analysis is also performed for Au patterns for comparison. Fig. 4 shows a cleaved and polished edge cross section of Au pattern after Re electrodeposition. As discussed previously, this is the most challenging case. Not only does the deposited

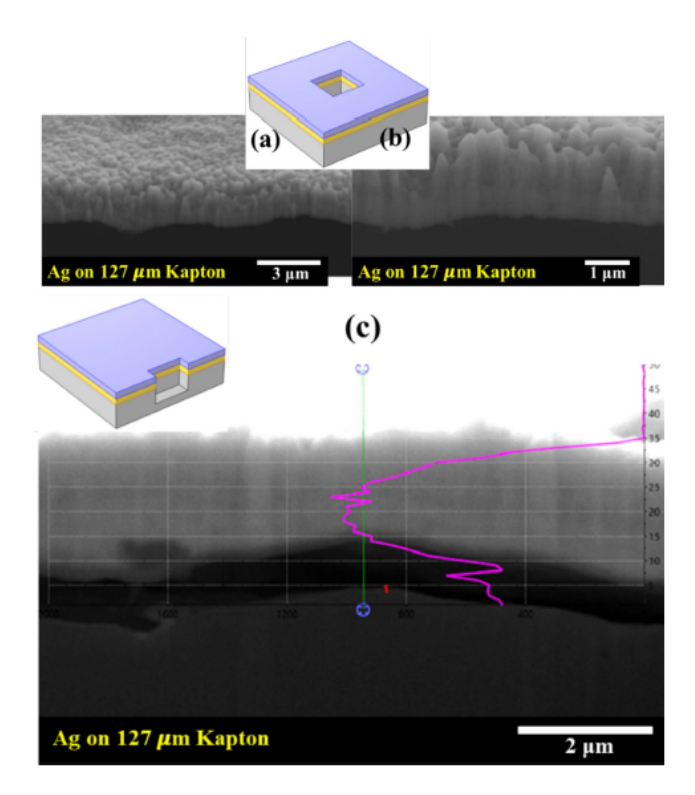


Fig. 3. SEM image of a cross section of AJP Ag layer on (a) and (b) Kapton in the Ag pattern and (c) polished at the cleaved edge of the Ag pattern. The insets show diagrams of the two different sectioning locations.

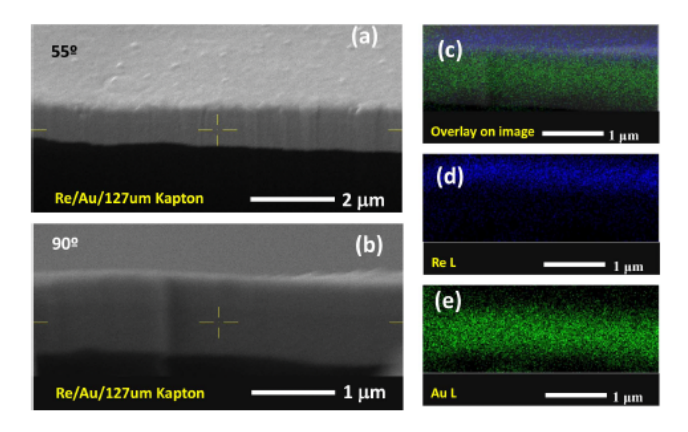


Fig. 4. (a) and (b) SEM images and (c)-(e) EDS elemental mapping of a polished cross section at the cleaved edge of electrodeposited Re on AJP Au layer on Kapton.

Re layer introduce internal stress and tend to delaminate the film but also mechanical stress is inevitable during the handling and cleaving, aggravating the delamination. However, a nearly perfectly adherent interface is observed between the metal and Kapton. In addition, the Re and Au interface is also clearly observed from the elemental mapping. While the analysis is not performed with high-resolution STEM, this absence of apparent intermixing is consistent with the reported negligible solubility of either metal element in the other [26]. This result is confirmed with another cross sectioning inside the pattern [illustrated by the inset in Fig. 3(b)] and a similar perfect interface is observed.

TABLE I RESISTANCE (Ω) OF AJP SEED LAYERS ON 127 μm Kapton

Seed layer	Specimen #1	Specimen #2	Specimen #3	Specimen#4
AJP Au on roughened Kapton	0.169	0.183	0.176	0.179
AJP Au on smooth Kapton	0.156	0.158	0.148	0.149
AJP Ag on roughened Kapton	0.029	0.026	0.030	0.028
AJP Ag on smooth Kapton	0.025	0.026	0.027	0.025

This cross-sectional characterization of the film stack clearly confirms the visual inspection of the different adhesions between Ag and Au. It is interesting that the two metals printed using similar chemistry and process result in such drastically different results. Some efforts have been devoted to find out the mechanism for this. For example, as mentioned earlier, a higher sintering temperature of 300 °C (instead of 120 °C) is used for printed Ag layers but fails to produce an adherent Re layer for further characterization. The preliminary thermal gravimetric analysis shown in Fig. S6 in Supplementary Information is carried out to characterize the mass loss during sintering due to solvent evaporation, but no clear difference is observed between Ag and Au, and further studies will be required to understand the difference between the two.

C. Film Resistance Measurements

Film resistance is measured in ambient using a four-probe setup on the 1 mm x 10 mm bar pattern. A small constant current of 10 mA is used for the measurements of a set of AJP seed layers on 1200 grit roughened Kapton and smooth Kapton. The results are presented in Table I.

The sheet resistance can be calculated from the measurements assuming parallel current flow. The measured resistance for printed Au layers ranges from 0.15 to 0.18 Ω . This corresponds to a sheet resistance between 0.075 and 0.09 Ω/sq . Considering the film thickness measured with profilometry for the Au layer ranging from 0.85 to 1.6 μm , this suggests a resistivity of AJP Au from 6.4 to 14.4 $\mu\Omega\cdot\text{cm}$, about 3–6.5 times higher than the intrinsic resistivity of Au metal (2.2 $\mu\Omega\cdot\text{cm}$). On the other hand, the printed Ag layers have a resistance of 0.025 to 0.030 Ω and a thickness of 3.2 to 4.0 μm . The corresponding resistivity is 4–6 $\mu\Omega\text{-cm}$ or 2.5–4 times higher than the bulk Ag metal. These observations are consistent with literature reports [27], [28].

The film resistance is also characterized after Re electrode-position on each type of substrate. The Re electrodeposition is carried out using the same process conditions, resulting in a reproducible thickness between 400 and 500 nm measured with XRF with small experimental variation from electrodeposition and XRF measurements. As shown in Table II, the resistance of the film stack slightly decreases after Re deposition due to the additional conductive path in Re. However, the overall resistance of the film is apparently dominated by the AJP seed layer (Au or Ag). The effect of the Re layer on top can theoretically be viewed as a conductive path in parallel with the seed. However, a quantitative calculation of this effect is not practical because

TABLE II RESISTANCE (Ω) of Electrodeposited Re on AJP Seed Layers on 127 μm Kapton

Substrate	Re thickness from		Resistance (Ω) after
	XRF (nm)	Re deposition	Re deposition
Au on roughened Kapton	496	0.169	0.164
Au on smooth Kapton	466	0.158	0.154
Ag on roughened Kapton	420	0.029	0.025
Ag on smooth Kapton	466	0.025	0.020

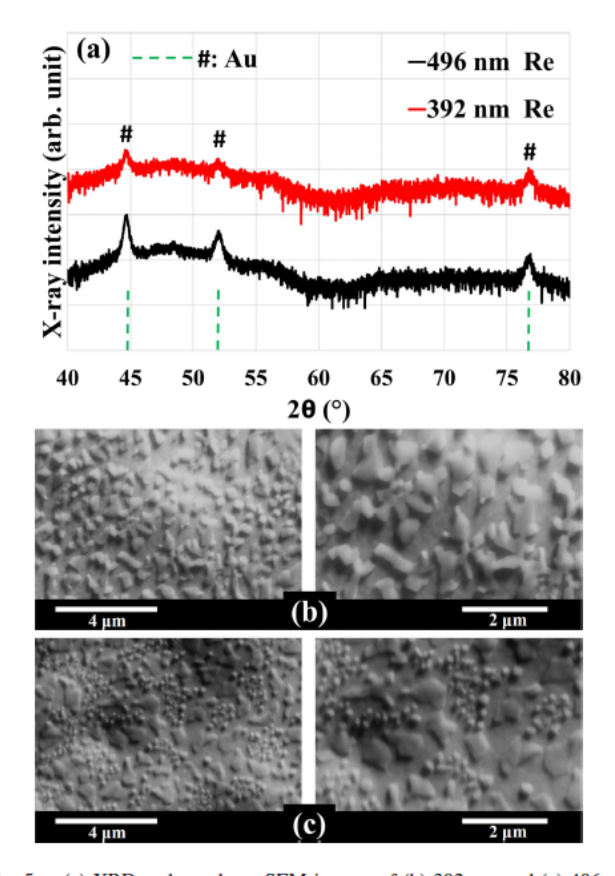


Fig. 5. (a) XRD and top-down SEM images of (b) 392-nm and (c) 496-nm Re films electrodeposited on Au printed on (b) smooth Kapton and (c) Kapton roughened with 1200 grit sandpaper.

the measurement variation is expected to overwhelm the effect of this much thinner Re metal layer.

D. Crystallographic Structure, Morphology, Composition, and Superconductivity

Fig. 5(a) shows the XRD patterns of electrodeposited Re on Au seed layer AJP on the Kapton. Two Re films, one on smooth Kapton and the other on Kapton roughened with 1200 grit sandpaper, are presented. Both samples are deposited at the same constant potential of -1 V for 300 s. The intensity on the y-axis is in the log scale to ease the comparison. The only strong sharp peaks, observed for both samples, are from Au. Broad background peaks at 2θ values between 40° and 55° are observed for both samples, corresponding to the amorphous structure of as-deposited Re, consistent with previous studies reported for Re films electrodeposited on rigid substrates [18], [19].

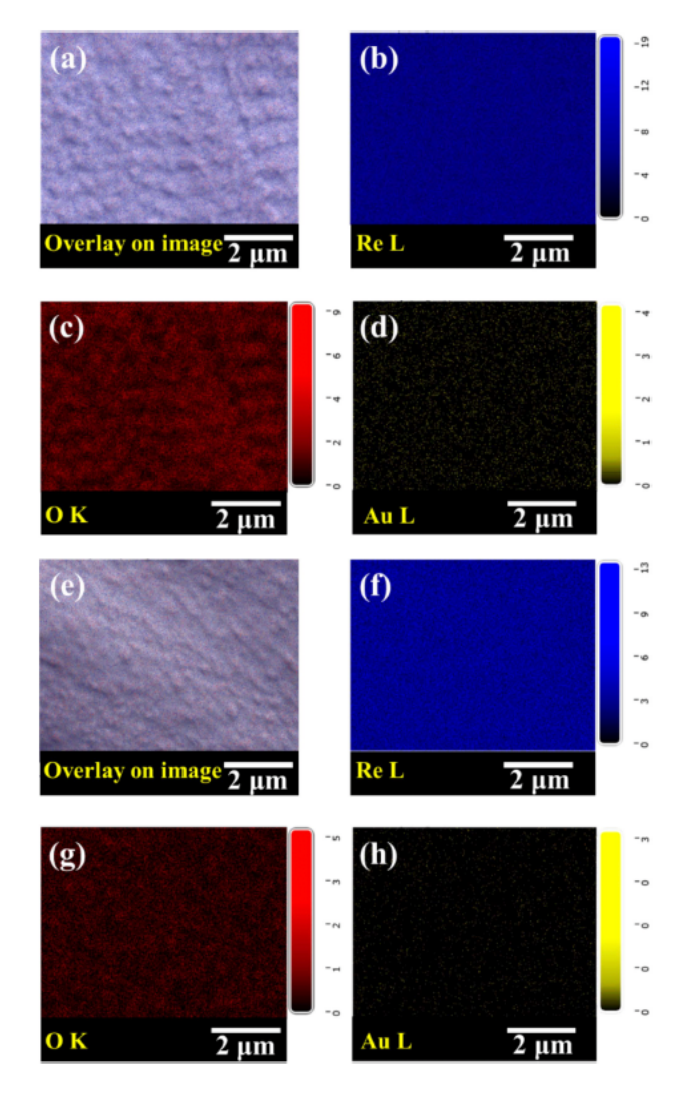


Fig. 6. SEM and the Re, O, Au elemental mapping of (a)—(d) 392-nm Re films electrodeposited on Au printed on smooth Kapton. (e)—(h) 496-nm Re films electrodeposited on Au printed on Kapton roughened with 1200 grit sandpaper. The contrasts of the elemental maps have been adjusted for better observation of eyes.

Fig. 5(b) and (c) shows the top-down SEM characterization of the same Re films, where an extremely smooth background surface with flat islands on top is observed for both films. Electrodeposited Re films on PVD Au layer on Si substrates were reported to be smooth [19]. It is believed that the morphology of electrodeposited Re films is strongly influenced by the AJP seed layer. This is not only because of the morphology of the seed layer itself but also because the Re nucleation and growth behavior on the printed seed can be completely different from on bulk metal or PVD seed on Si. The top-down SEM images of a typical AJP Au film is provided at the same magnification in Fig. S7 in Supplementary Information. The AJP Au is extremely smooth with little to no features observed.

Further microscopic analysis with EDS elemental mapping is carried out to determine if these islands are different from the background. It is worth noting that with the naked eye, these films appear metallic silver in color despite the presence of

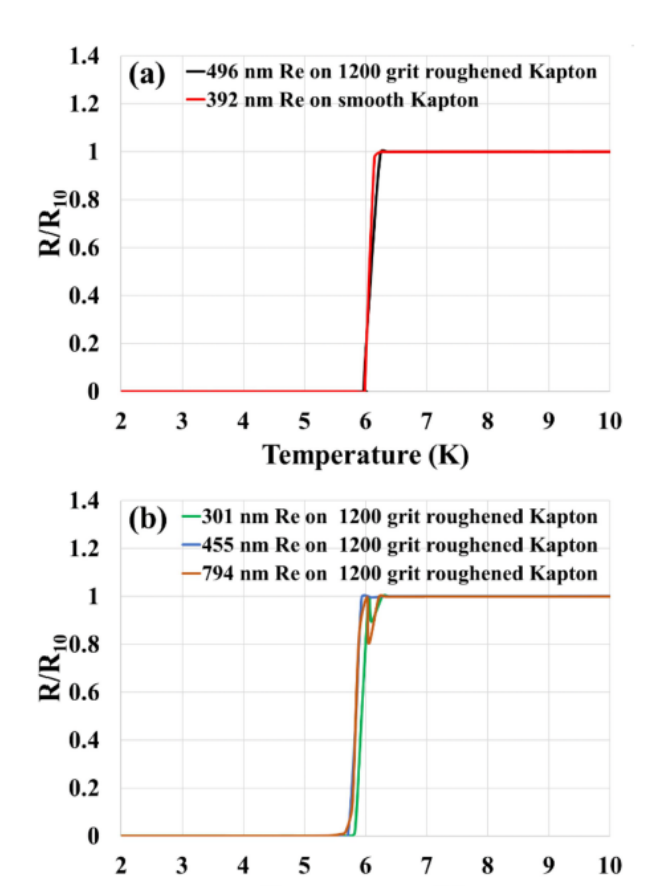


Fig. 7. Superconducting transition of (a) two Re films deposited on Au on roughened and smooth Kapton, and (b) three additional Re films deposited on Au on 1200 grit roughened Kapton.

Temperature (K)

particles or islands under SEM. Fig. 6 shows the results for these two films. The contrast of the elemental maps has been adjusted for easier observation of patterns. Under the typical resolution of EDS, i.e., about 1 μm, Re and Au are uniformly distributed with no obvious patterns. However, the islands correlate well with the oxygen signal, suggesting a higher oxygen content in the islands. It is known that surface topography can contribute to signal intensity variation due to shadowing [29], [30] and surface oxidation can easily occur after deposition. It requires future work to better understand the chemical composition of these islands, whether or not certain types of rhenium oxides form, and if so, at what condition and how fast such oxides form.

Despite the higher oxygen content of those islands on the Re surface, the superconducting transition behaviors of Re films seem to be barely impacted. The same two films shown in Figs. 5 and 6 are characterized in PPMS for sheet resistance with temperature sweep. As shown in Fig. 7(a), a very sharp transition is observed between 6.2 and 6.0 K. Bulk crystalline Re has a transition temperature, or critical temperature (T_c), of 1.8 K [31], [32]. This much improved T_c of about 6 K is known due to the amorphous structure for electrodeposited Re [17], [18], [19]. This T_c is above the boiling point of liquid helium and is considered a first successful demonstration of such improved

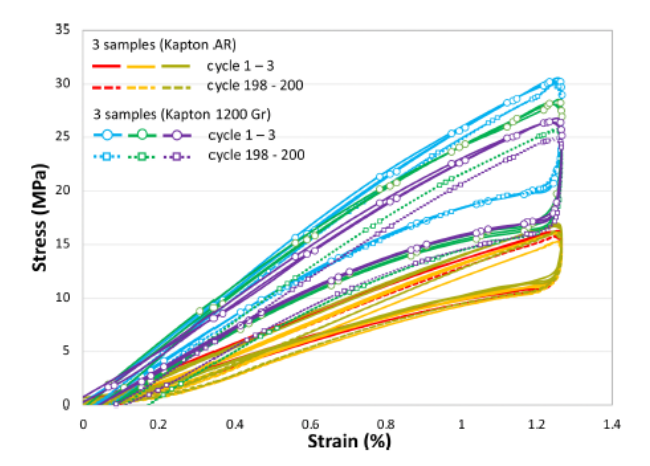


Fig. 8. Cycling testing of electrodeposited Re on printed Au seed layers on Kapton substrates. The solid and dashed lines without markers are for layers on as-received (AR) Kapton substrates without sandpaper modification, and the curves with markers are for layers on Kapton substrates roughened with 1200 grit sandpaper.

 T_c of electrodeposited Re on flexible substrates. In addition to these two films, multiple Re films have been deposited in the same conditions on Au printed on roughened Kapton and the resistance measurement has been repeated with the results shown in Fig. 7(b). All films show sharp rapid transitions between 5.8 and 6.1 K. These results demonstrate the good reproducibility of the improved superconductivity of electrodeposited Re on flexible substrates.

E. Flexure Testing

Fig. 8 shows the cycling testing of electrodeposited Re films with thicknesses between 400 nm and 500 nm on AJP Au on Kapton. Both unmodified Kapton and 1200 grit roughened Kapton are included in the testing, with three duplicated specimens in each case. These samples are tested with cyclic three-point bending for 200 cycles to a strain of 1.27%. While a maximum stress of 15 MPa at 1.27% is recorded for the Re-Au stacks on unmodified Kapton substrates, a maximum stress of 26-30 MPA is observed for the Re films on AJP Au on 1200 grit roughened substrates. These results are identical to the data obtained with the same tests on the AJP Au seed on Kapton before Re electrodeposition, shown in Fig. S9 in Supplementary Information. In addition, Fig. S8 in the Supplementary Information presents the single three-point bend test result for bare Kapton. It can be seen that the stress-strain relationship for the Kapton substrate is almost identical to the cases with Au or Au-Re metals before a 1.27% strain is reached. A comparison of these results shows the addition of the metal layers has no observable effects on the flexure properties of the stack. Furthermore, the results on smooth Kapton in Fig. 8 show all three samples are in good agreement with each other with a strong overlap. A significant divergence can be seen between the three roughened Kapton samples with variations between 15% and 20%. This suggests that surface roughening significantly increases the rigidity of Kapton and that the experimental variation in the roughening step results in the variation in flexibility.

V. CONCLUSION

The compatibility of aerosol jet printing of a metal seed layer with the electrodeposition of Re on Kapton is found to be a viable means of producing flexible superconducting film. Numerous efforts with printed Ag seed to get adhered Re-Ag composites on Kapton are found to be unsuccessful. On the other hand, electrodeposition of Re from a water-in-salt electrolyte onto the AJP Au seed layer on Kapton shows excellent reproducibility. Such electrodeposited Re films do not degrade the overall sheet conductivity of the stack composites. A sharp superconducting transition between 5.8 K and 6.2 K on the highly flexible Kapton is measured, establishing this composite film stack as a high-performing, low-cost, light, flexible, and modular superconducting alternate to the current state-of-the-art. The flexure tests indicate that the addition of Au and Re has no observable effect on the mechanical properties of the entire stack and the properties are solely dictated by the flexible substrate.

ACKNOWLEDGMENT

The authors would like to thank The Alabama Analytical Research Center, College of Engineering Analytical Facility, and Arts and Science College Glass Shop at the University of Alabama for characterization and for making the parts used in this study.

REFERENCES

- [1] F. Bova, A. Goldfarb, and R. G. Melko, "Commercial applications of quantum computing," *EPJ Quantum Technol.*, vol. 8, no. 1, Jan. 2021, Art. no. 2, doi: 10.1140/epjqt/s40507-021-00091-1.
- [2] Y. Cao et al., "Quantum chemistry in the age of quantum computing," Chem. Rev., vol. 119, no. 19, pp. 10856–10915, Oct. 2019, doi: 10.1021/acs.chemrev.8b00803.
- [3] R. Orús, S. Mugel, and E. Lizaso, "Quantum computing for finance: Overview and prospects," *Rev. Phys.*, vol. 4, Nov. 2019, Art. no. 100028, doi: 10.1016/j.revip.2019.100028.
- [4] V. Hassija, V. Chamola, A. Goyal, S. S. Kanhere, and N. Guizani, "Forthcoming applications of quantum computing: Peeking into the future," *IET Quantum Commun.*, vol. 1, no. 2, pp. 35–41, 2020, doi: 10.1049/iet-qtc.2020.0026.
- [5] A. Kumar and S. Garhwal, "State-of-the-art survey of quantum cryptography," Arch. Comput. Methods Eng., vol. 28, no. 5, pp. 3831–3868, Aug. 2021, doi: 10.1007/s11831-021-09561-2.
- [6] S. Krinner et al., "Engineering cryogenic setups for 100-qubit scale superconducting circuit systems," EPJ Quantum Technol., vol. 6, no. 1, 2019, Art. no. 2.
- [7] J. Li et al., "Printable two-dimensional superconducting monolayers," Nature Mater., vol. 20, no. 2, pp. 181–187, 2021.
- [8] L. Ren et al., "Nanodroplets for stretchable superconducting circuits," Adv. Funct. Mater., vol. 26, no. 44, pp. 8111–8118, 2016.
- [9] D. B. Tuckerman et al., "Flexible superconducting Nb transmission lines on thin film polyimide for quantum computing applications," *Supercond. Sci. Technol.*, vol. 29, no. 8, 2016, Art. no. 084007.
- [10] V. Solovyov, O.-P. Saira, Z. Mendleson, and I. Drozdov, "YBCO-on-Kapton: Material for high-density quantum computer interconnects with ultra-low thermal loss," *IEEE Trans. Appl. Supercond.*, vol. 31, no. 5, Aug. 2021, Art. no. 1700105, doi: 10.1109/tasc.2021.3057010.
- [11] N. Wilkinson, M. Smith, R. Kay, and R. Harris, "A review of aerosol jet printing—A non-traditional hybrid process for micro-manufacturing," *Int. J. Adv. Manuf. Technol.*, vol. 105, no. 11, pp. 4599–4619, 2019.

- [12] M. J. Aus, B. Szpunar, U. Erb, G. Palumbo, and K. T. Aust, "Electrical, magnetic and mechanical properties of nanocrystalline nickel," MRS Online Proc. Library, vol. 318, no. 1, pp. 39–44, Dec. 1993, doi: 10.1557/PROC-318-39.
- [13] H. Deligianni, S. Ahmed, and L. T. Romankiw, "The next frontier: Electrodeposition for solar cell fabrication," *Interface Mag.*, vol. 20, no. 2, pp. 47–53, 2011, doi: 10.1149/2.f06112if.
- [14] T. P. Moffat and D. Josell, "Superconformal electrodeposition for 3-dimensional interconnects," *Isr. J. Chem.*, vol. 50, no. 3, pp. 312–320, 2010, doi: 10.1002/jich.201000029.
- [15] H. Nakano, H. Suzuki, T. Haba, H. Yoshida, A. Chinda, and H. Akahoshi, "Advanced trench filling process by selective copper electrodeposition for ultra fine printed wiring board fabrication," in *Proc. 60th Electron. Com*pon. Technol. Conf., 2010, pp. 612–616, doi: 10.1109/ectc.2010.5490865.
- [16] L. Tsui, S. C. Kayser, S. A. Strong, and J. M. Lavin, "High resolution aerosol jet printed components with electrodeposition-enhanced conductance," ECS J. Solid State Sci. Technol., vol. 10, no. 4, 2021, Art. no. 047001.
- [17] D. P. Pappas et al., "Enhanced superconducting transition temperature in electroplated rhenium," Appl. Phys. Lett., vol. 112, no. 18, 2018, Art. no. 182601, doi: 10.1063/1.5027104.
- [18] W. D. Sides, E. Hassani, D. P. Pappas, Y. Hu, T.-S. Oh, and Q. Huang, "Grain growth and superconductivity of rhenium electrodeposited from water-in-salt electrolytes," *J. Appl. Phys.*, vol. 127, no. 8, 2020, Art. no. 085301, doi: 10.1063/1.5139909.
- [19] Q. Huang and Y. Hu, "Electrodeposition of superconducting rhenium with water-in-salt electrolyte," J. Electrochem. Soc., vol. 165, no. 16, pp. D796–D801, Jan. 2018, doi: 10.1149/2.0261816jes.
- [20] Q. Huang and T. W. Lyons, "Electrodeposition of rhenium with suppressed hydrogen evolution from water-in-salt electrolyte," *Electrochem. Commun.*, vol. 93, pp. 53–56, 2018, doi: 10.1016/j.elecom.2018.06.003.
- [21] S. H. Pawar, R. S. Nimbalkar, M. M. Tonape, and V. N. Shinde, "Y-Ba-Cu-O superconducting wires via electrodeposition process," *Indian J. Cryogenics*, vol. 18, no. 1–4, pp. 79–86, 1993. [Online]. Available: http://inis.iaea.org/search/search.aspx?orig_q=RN:28012305
- [22] R. N. Bhattacharya et al., "Superconducting thallium oxide films by the electrodeposition method," *Physica C, Supercond.*, vol. 304, no. 1, pp. 55-65, Aug. 1998, doi: 10.1016/S0921-4534(98)00277-9.
- [23] R. N. Bhattacharya et al., "Superconducting epitaxial (TlBi)_{0.9}Sr_{1.6}Ba_{0.4}Ca₂Cu₃Ag_{0.2}O_x film from an electrodeposited precursor," *Electrochem. Solid-State Lett.*, vol. 1, no. 4, Aug. 1998, Art. no. 165, doi: 10.1149/1.1390673.
- [24] P.-S. Tape and T. Paint, Standard Test Methods For Measuring Adhesion By Tape Test. West Conshohocken, PA, USA: ASTM International, 2012.
- [25] S. Hadian and D. Gabe, "Residual stresses in electrodeposits of nickel and nickel-iron alloys," Surf. Coatings Technol., vol. 122, no. 2/3, pp. 118–135, 1999.
- [26] J. Niemiec, "The system gold-rhenium," *Roczniki Chem.*, vol. 32, pp. 619–620, 1956.
- [27] D. Zhao, T. Liu, J. G. Park, M. Zhang, J.-M. Chen, and B. Wang, "Conductivity enhancement of aerosol-jet printed electronics by using silver nanoparticles ink with carbon nanotubes," *Microelectron. Eng.*, vol. 96, pp. 71–75, 2012.
- [28] A. Mahajan, C. D. Frisbie, and L. F. Francis, "Optimization of aerosol jet printing for high-resolution, high-aspect ratio silver lines," ACS Appl. Mater. Interfaces, vol. 5, no. 11, pp. 4856–4864, 2013.
- [29] T. Rönnhult, B. Brox, and G. Fritze, "The influence of surface topography on the X-ray intensity in electron microprobe analysis (EDS/WDS)," *Scanning*, vol. 9, no. 2, pp. 81–87, 1987.
- [30] F. Hess, R. Falk, and D. Bayer, "The influence of specimen topography on X-ray microanalysis element mapping," *Amer. J. Botany*, vol. 62, no. 3, pp. 246–253, 1975.
- [31] J. K. Hulm, "Superconductivity of pure metallic rhenium," *Phys. Rev.*, vol. 94, no. 5, pp. 1390–1391, 1954, doi: 10.1103/physrev.94.1390.2.
- [32] J. K. Hulm and B. B. Goodman, "Superconducting properties of rhenium, ruthenium, and osmium," *Phys. Rev.*, vol. 106, no. 4, pp. 659–671, 1957, doi: 10.1103/physrev.106.659.